A comparison of radiative transfer models for simulating Atmospheric Infrared Sounder (AIRS) radiances

R. Saunders,[1] P. Rayer,[1] P. Brunel,[2] A. von Engeln,[3] N. Bormann,[4] L. Strow,[5] S. Hannon,[5] S. Heilliette,[6] Xu Liu,[7] F. Miskolczi,[7] Y. Han,[8] G. Masiello,[9] J.-L. Moncet,[10] Gennady Uymin,[10] V. Sherlock,[11] and D. S. Turner[12]

Received 17 January 2006; revised 6 June 2006; accepted 17 July 2006; published 4 January 2007.

[1] A comparison of radiative transfer models for simulating radiances from the Atmospheric Infrared Sounder (AIRS), has been undertaken. Results from 14 line-by-line and fast parameterized infrared models were submitted. Several aspects of the models were compared. First, the forward model calculations for all 2378 AIRS channels for 52 diverse atmospheric profiles and one tropical Pacific profile coincident with AIRS data were performed for three local zenith viewing angles: nadir, 45, and 60 degrees. Second, for a subset of the models and only 20 AIRS channels the transmittances from each layer to space were provided. Finally, for some models the Jacobians with respect to temperature, water vapor, and ozone were also computed. For the forward model calculations, most models agree to within 0.02 K when compared to a reference line-by-line model averaged over a subset of profiles, with the exception of a few spectral regions. When compared with AIRS observations, however, the mean differences increase to 0.2 K, and for a few models even greater differences are seen. The transmittance differences highlighted regions of the spectrum where the spectroscopy of the models differs, particularly in the carbon dioxide absorption bands at 667 cm^{-1} and 2386 cm^{-1}. For the Jacobians all models have some profiles/channels that do not fit the reference well, and the main problems are documented here. The model differences only increase slightly for off-nadir viewing angles for both forward and Jacobian calculations.

Citation: Saunders, R., et al. (2007), A comparison of radiative transfer models for simulating Atmospheric Infrared Sounder (AIRS) radiances, *J. Geophys. Res.*, *112*, D01S90, doi:10.1029/2006JD007088.

1. Introduction

[2] Fast radiative transfer (RT) models are now an integral component of any numerical weather prediction (NWP) model assimilating satellite radiances or using radiances for model validation purposes. Given the significant impacts of radiances in NWP model forecasts [*Andersson et al.*, 1994; *English et al.*, 2000] it is important that we strive to develop fast RT models which achieve the required level of accuracy while at the same time having error characteristics which are well understood. In this way the impact of the satellite radiances on the NWP analyses can be optimized. Ideally the errors in the RT forward model used for assimilation should be small relative to the instrument noise and uncorrelated. Fast RT models are also important for providing retrievals of the atmospheric state for climate data sets and providing simulated satellite data sets from NWP model fields. For both assimilation and retrieval applications it is important to emphasize that it is not only the forward model calculations (i.e., top of atmosphere radiances computed from a given atmospheric state) which are significant but also the gradients of the RT model radiances with respect to the profile variables strictly referred to as the Jacobian (but see later) and defined as

$$\mathbf{H} = \frac{\partial \boldsymbol{y}}{\partial \boldsymbol{X}} \tag{1}$$

where $\boldsymbol{y}$ is the vector of channel radiances (2378 for Atmospheric Infrared Sounder (AIRS)), $\boldsymbol{X}$ is the vector of atmospheric state variables (typically dimensions of number of levels $\times$ number of active gases plus a few surface variables which for this study came to $\sim$310) and $\mathbf{H}$ is the Jacobian matrix with dimensions of $\boldsymbol{y}$ by $\boldsymbol{X}$. It is the

[1]Met Office, Exeter, UK.
[2]MétéoFrance, CMS, Lannion, France.
[3]Institute of Environmental Physics, Bremen University, Bremen, Germany.
[4]European Centre for Medium Range Weather Forecasts, Reading, UK.
[5]Department of Physics, University of Maryland Baltimore County, Baltimore, Maryland, USA.
[6]CNRS, Laboratoire Meteorologie Dynamique, Palaiseau, France.
[7]NASA Langley Research Center, Hampton, Virginia, USA.
[8]NOAA/NESDIS, Camp Springs, Maryland, USA.
[9]IMAA-CNR, Tito Scalo, Potenza, Italy.
[10]Atmospheric and Environmental Research, Incorporated, Lexington, Massachusetts, USA.
[11]National Institute of Water and Atmospheric Research, Wellington, New Zealand.
[12]Met Service Canada, Downsview, Ontario, Canada.

Table 1. Fast Models Which Participated in the Comparison

Model Name and Reference	Base Model Spectroscopy Water Vapor Continuum Line Mixing	Participant	Results Submitted Transmittances/Jacobian	Method
RTTOV-7 [*Saunders et al.*, 1999]	GENLN2v2 Hitran-96 CKD2.1 [*Strow et al.*, 1994]	R. Saunders, Met Office	Yes/Analytic	Regression
RTTOV-8 [*Saunders et al.*, 1999]	kCARTA (1.11)[a] Hitran-2004 Modified MTCKD 1.0 [*DeSouza-Machado et al.*, 1999]	R. Saunders, P. Brunel, Met Office	Yes/Analytic	Regression
Optran v7 [*Xiong and McMillin*, 2005; *McMillin et al.*, 2005]	LBLRTM v7.04 HITRAN-2000 MTCKD 1.0 [*Hoke et al.*, 1989]	Y. Han, NESDIS	Yes/Analytic	Regression
OSS [*Moncet et al.*, 2004]	LBLRTMV8.3 HITRAN-2000 MTCKD 1.0 [*Hoke et al.*, 1989]	J.-L. Moncet, G. Uymin, AER	None/Analytic	Precomputed LUT
σ-IASI [*Amato et al.*, 2002]	LBLRTMV8.1 HITRAN-2000 MTCKD 1.0 [*Hoke et al.*, 1989]	G. Masiello, C. Serio, DIFA, UniBas	Yes/Analytic	Precomputed LUT
Gastropod 0.3.0 [*Sherlock et al.*, 2003]	kCARTA 2000[a] Hitran-1998[b] CKD2.4 [*Strow et al.*, 2003]	V. Sherlock, NIWA	Yes/Analytic	Regression
SARTAv 1.05 [*Strow et al.*, 2003]	kCARTA (1.07)[a] Hitran-2000 Modified MTCKD 1.0 [*DeSouza-Machado et al.*, 1999]	S. Hannon, L. Strow, UMBC	None/None	Regression
PCRTM *Liu et al.*, 2006]	LBLRTM v8.3 Hitran-2000 MTCKD 1.0 [*Hoke et al.*, 1989]	Xu Liu, NASA, LaRC	Yes/Analytical	LUT/Regression

[a]kCARTA is described in *Strow et al.* [1998].
[b]Includes the Toth H_2O lines.

Jacobian which allows increments in "radiance space" to be mapped back into increments in model state variables, assuming linearity about the model state $\boldsymbol{X}$, thereby bringing the NWP model state closer to the radiance observations.

[3] Several years ago comparisons of radiative transfer (RT) models for ATOVS (Advanced TIROS Operational Vertical Sounder) infrared and microwave channels were made [*Soden et al.*, 2000; *Garand et al.*, 2001] that helped to better define the radiative transfer modeling errors for ATOVS. More recently, with the advent of high spectral resolution infrared sounders, e.g., Atmospheric Infrared Sounder (AIRS) and Infrared Atmospheric Sounding Interferometer (IASI), enhanced versions of the fast ATOVS radiative transfer models have evolved to include simulations of these sounders. The success of the AIRS spectrometer in providing very stable high spectral resolution top of atmosphere infrared radiances has provided an impetus to improve and assess the RT modeling for atmospheric sounding applications in the thermal infrared. A recent study by *Tjemkes et al.* [2003] comparing line-by-line RT models for IASI simulations has also helped quantify the errors in the line-by-line models.

[4] This AIRS radiative transfer model comparison was proposed at the first workshop for Soundings from High Spectral Resolution Observations at Madison, Wisconsin in May 2003, and was undertaken under the auspices of the International TOVS Working Group. The aims of the intercomparison were defined to be (1) to compare the forward model calculations for all AIRS channels for a set of diverse atmospheric profiles and one tropical Pacific profile coincident with AIRS data; (2) to compare the profile transmittances for a representative subset of 20 channels; and (3) to compare temperature, water vapor and ozone Jacobians from each model for these 20 channels. The results from this study would then allow the error characteristics of AIRS fast RT models to be better estimated for retrieval and data assimilation applications and to compare them with the AIRS instrument noise. In the process of this comparison exercise, several models had problems identified in their implementation as a result of the comparison and they were able to be corrected before the final analysis was undertaken.

[5] The paper is structured as follows: section 2 describes the models submitted, section 3 the details of the comparison process, section 4 the results for the forward model comparisons, section 5 the results for the transmittances and Jacobians, and section 6 summarises the conclusions of the intercomparison and identifies areas requiring further study.

2. Models Submitted

[6] The 14 radiative transfer models that participated in this study are listed in Tables 1 and 2 together with references for each model. All models provided brightness temperatures for all 2378 AIRS channels for 3 viewing angles and for the 52 diverse atmospheres. The comparison was performed in terms of equivalent black body brightness temperatures for ease of interpretation although this does introduce a small additional uncertainty through the assumptions made in the conversion from radiance to brightness temperature. In addition, one profile from the Western Tropical Pacific Atmospheric Radiation Measurement (ARM) site coincident with an AIRS observation was also modeled by all the participants. Results were submitted for three viewing angles, 0, 45, and 60 degrees surface incidence, for the European Centre for Medium-Range Weather Forecasts (ECMWF) model profile simulations, and at the AIRS viewing angle (11.56 degrees) for the tropical ARM site profile.

[7] Table 1 lists the participating fast models. These models sacrifice accuracy for speed of computation to enable calculations to be made in real time as the AIRS radiances are received. For simplicity they can be regarded as being in two classes: those using regression techniques on the profile variables and those employing precomputed look up tables (LUT). The references in Table 1 give

Table 2. Line-by-Line Models Which Participated in the Comparison

Model Name and Reference	Base Model Spectroscopy Water Vapor Continuum Line Mixing	Participant	Results Submitted Transmittances/Jacobian	Method
RFM (http://www.atm.ox.ac.uk/RFM)	GENLN2 HITRAN-2000 CKD2.4 [*Strow et al.*, 1994]	N. Bormann, ECMWF	Yes/Finite diff	Full LbL computation
LBLRTM v8.3 [*Clough et al.*, 1992]	HITRAN-2000 MTCKD 1.0 [*Hoke et al.*, 1989]	J.-L. Moncet, AER	None/Finite diff	Full LbL computation
ARTS 1.0.136 [*Buehler et al.*, 2005]	HITRAN-2003 MTCKD 1.0 None	A. von Engeln, Bremen	None/None	Full LbL computation
4A [*Scott and Chedin*, 1981], (http://www.noveltis.net/4AOP/)	STRANSAC GEISA 2001 [*Rodriguez et al.*, 1999]	S. Heilliette, LMD	Yes/Analytic	Precomputed LUT
FLBL-3 [*Turner*, 1995]	HITRAN-2001 CKD2.4 [*Strow et al.*, 1998]	D.S. Turner, MSC	Yes/Analytic	Precomputed LUT
HARTCODE [*Miskolczi et al.*, 1989]	HITRAN-2000 CKD2.4 [*Rodriguez et al.*, 1999]	F. Miskolczi, NASA, LaRC	None/None	Full LbL computation

descriptions of the individual models and the methods used to enable fast simulations.

[8] Table 2 lists the line by line models with their references. For most of these models the full transmittance calculation at a particular frequency is computed using the line parameters from a spectroscopic database and an assumed line shape plus continuum absorption parameterisation. Two of the models in Table 2 use large precomputed look up tables but cannot be regarded as fast models. A subset of the models indicated in Tables 1 and 2 also computed layer to space transmittances and temperature, water vapor and ozone Jacobians for 20 representative AIRS channels listed in Table 3.

3. Definition of Comparison

[9] The process by which the comparison was undertaken is described in this section.

3.1. Profile Data Sets

[10] The profiles were extracted from the diverse set of 13495 profiles generated from the ECMWF 40 year reanalysis, ERA-40. The methodology for extracting a small number of profiles (49 in this case) to represent the full variability of the atmosphere in temperature, water vapor and ozone is described by *Chevallier et al.* [2000] and the full characteristics of the ERA-40 data set are described by *Chevallier* [2001]. The profile data set used and corresponding surface parameters are available from the following web site: http://www.metoffice.gov.uk/research/interproj/nwpsaf/rtm/. The profiles were provided to participants on 101 levels defined by the AIRS science team. These levels were originally derived by evaluating

$$P(x) = \left(ax^2 + bx + c\right)^{7/2} \quad (2)$$

given that $P = 0.005$ hPa, $P = 300.0$ hPa, $P = 1100.0$ hPa, when $x = 1$, $x = 38$, $x = 101$ respectively, and values of the three coefficients are $a = -1.55 \times 10^{-4}$, $b = -5.59 \times 10^{-2}$, $c = 7.45$. These levels define a set of 100 layers with the depth decreasing from several km at the top to less than 200m at the surface. The ERA-40 model-based profiles only reach to 0.1 hPa. To extend them to the top of the 101 level set at 0.005 hPa, data from the Halogen Occultation Experiment (HALOE), which used solar occultation to measure simultaneous vertical profiles of temperature and various gases, were used. This was imposed above 5 hPa for water vapor and above 0.1 hPa for temperature, while a linear extrapolation in pressure of the top model value was used to extend the ozone profile. Some of the profiles lie above elevated land or icecaps and the surface pressure indicates this. The convention adopted for the subsurface levels was to maintain constant values of temperature, relative humidity, and ozone abundance below the surface. The model calculations assumed the surface was defined by the surface pressure which was provided.

[11] The characteristics of the 49 profiles used here are summarised in Figure 1 and Table 4. The use of model-based profiles ensured that the temperature profile was everywhere consistent with the abundance of both water vapor and ozone. Profiles 50–52 are synthetic and contain the adjusted minimum, adjusted maximum and mean profiles of the variables in the 13495-profile data set respectively. Model simulation results were submitted for the artificially extreme profiles (50, 51), but they are not included in this analysis as they are not a fair test of the models in realistic atmospheric conditions. Profile interpolation software was provided for those models not using the

Table 3. AIRS Channels Used for Transmittance and Jacobian Comparisons[a]

Channel Number	AIRS Channel	Frequency, cm^{-1}	Jacobian Computed
1	71	666.7	T
2	77	668.2	T
3	305	737.1	T
4	453	793.1	T, Q
5	672	871.2	T, Q
6	787	917.2	T
7	1021	1009.2	T, O_3
8	1090	1040.1	O_3
9	1142	1074.3	Q
10	1437	1323.8	Q
11	1449	1330.8	Q
12	1627	1427.1	Q
13	1766	1544.3	Q
14	1794	1563.5	Q
15	1812	1576.1	Q
16	1917	2229.3	T
17	1958	2268.7	T
18	1995	2305.5	T
19	2107	2385.9	T
20	2197	2500.3	T

[a]AIRS: Atmospheric Infrared Sounder.

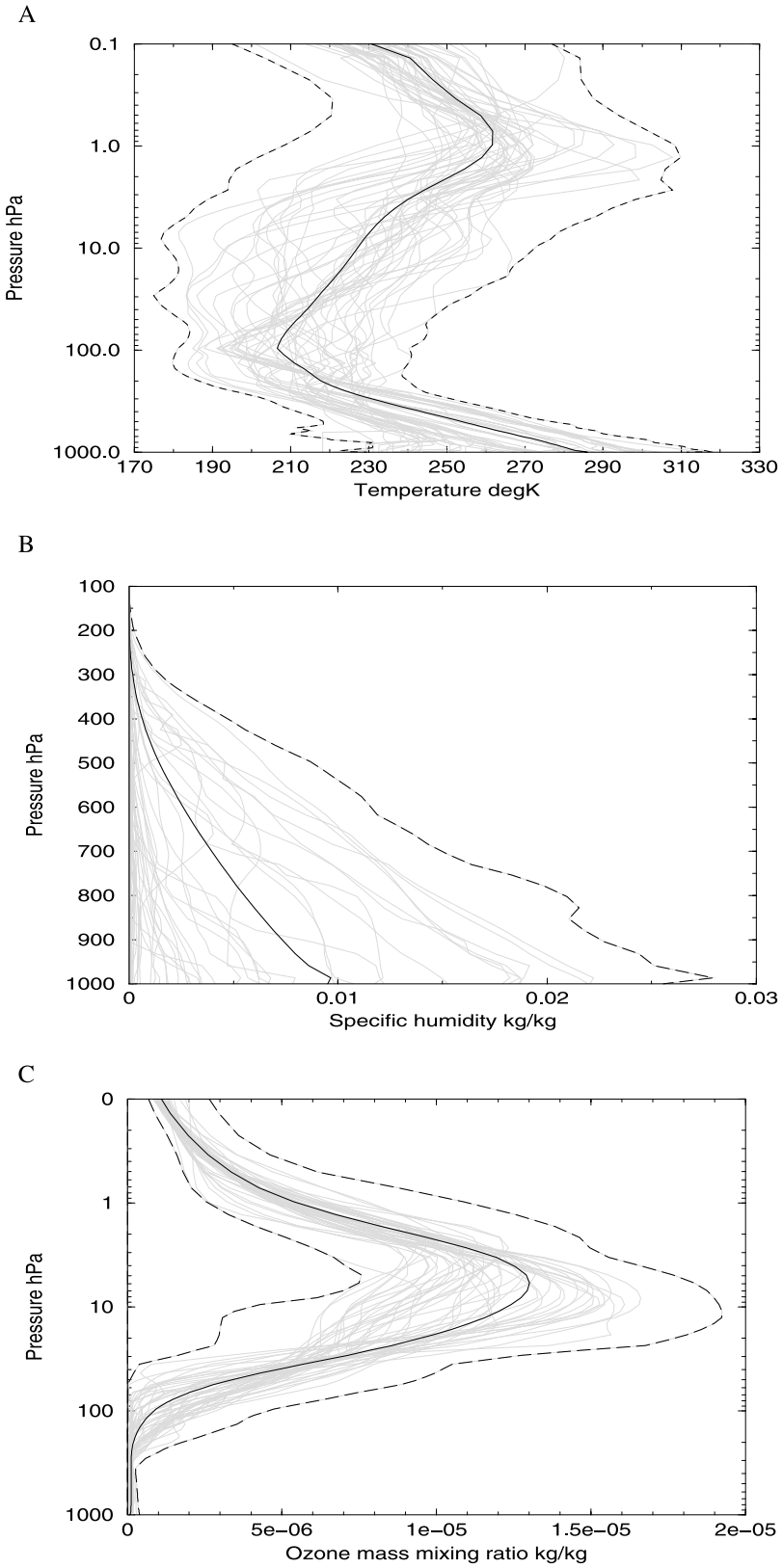

Figure 1. The ERA-40 diverse profiles used for the comparisons. The extreme profiles (not included in the results) are indicated by dashed lines and the profile mean by the thicker line. Plots for temperature, water vapor and ozone are shown.

Table 4. Characteristics of 49 Profiles Used for Comparison

Profile	Ps, hPa	Ts, K	Total Column Water, Kg/sq m	Total Ozone, DU
1	972.2	334.3	36.1	273.6
2	970.5	273.3	11.5	390.1
3	1049.4	240.2	0.6	364.2
4	1030.9	289.5	22.2	281.3
5	628.1	214.2	0.4	273.2
6	1005.0	302.1	76.7	264.7
7	1009.8	293.7	44.0	305.1
8	983.0	281.9	22.9	280.5
9	871.7	240.5	0.9	217.0
10	1018.9	255.7	2.8	419.1
11	1016.8	273.0	15.4	298.7
12	976.9	267.3	9.4	360.7
13	1011.4	236.1	0.8	427.1
14	870.8	231.7	0.3	288.4
15	991.5	262.3	7.0	223.2
16	1015.6	298.9	58.3	249.3
17	987.6	279.7	8.2	335.4
18	1029.1	284.8	8.2	276.2
19	833.9	249.7	2.0	234.1
20	841.0	228.1	0.5	261.9
21	1007.4	302.6	91.2	220.4
22	870.8	252.4	2.7	347.6
23	806.6	259.1	5.6	312.6
24	804.7	241.4	1.2	286.0
25	1001.5	315.0	57.2	274.4
26	968.3	298.6	90.5	283.8
27	846.4	235.2	0.5	300.3
28	993.6	243.9	2.0	243.8
29	1022.2	275.5	4.9	376.0
30	993.0	274.4	7.9	375.3
31	1006.8	287.1	44.2	284.3
32	824.9	230.3	0.2	302.1
33	1008.0	300.4	74.2	252.8
34	949.4	233.6	1.1	314.3
35	1014.5	293.6	20.8	298.6
36	1008.8	302.7	93.3	238.2
37	989.2	272.3	8.0	296.8
38	1004.7	215.2	0.3	377.5
39	1011.8	291.5	17.8	329.8
40	989.4	296.0	81.6	254.4
41	975.9	272.0	3.7	426.4
42	1022.2	275.1	4.4	292.4
43	996.3	273.1	11.6	304.1
44	977.3	273.8	7.4	334.8
45	1017.1	297.7	34.6	265.1
46	885.1	230.4	1.0	192.7
47	1017.7	276.0	20.3	258.0
48	803.1	232.2	0.4	301.0
49	1013.4	228.5	1.0	436.8
Mininum	1013.3	234.0	0.1	59.2
Maximum	1013.3	305.8	123.4	825.1
Mean	1013.3	286.5	36.1	303.2

AIRS 101 levels. For the surface the supplied skin temperature and a constant emissivity of 0.99 was assumed and the radiance of space set to zero ensuring the surface reflection effects as calculated by each model were included in the calculations. Solar effects were not included in the comparison. For other gases all modelers were asked to assume their own default profiles. RTTOV-8 uses the 52 profiles as its dependent set for training the model coefficients and so for this model the results are not independent.

[12] For the profile coincident with the AIRS measurements on 8 December 2002 over the tropical Pacific ARM site at 0.5°S; 167°E the temperature (below 60 hPa) and water vapor (below 200 hPa) profiles were taken from a radiosonde. ECMWF analyses provided the surface pressure, temperature above 60 hPa, water vapor above 200 hPa and ozone profile. The radiative skin temperature was from a retrieval using the AIRS window channels. The total column CO amount was adjusted empirically to best fit the measured radiance data. The AIRS zenith angle at the surface was 11deg at the ARM site.

3.2. AIRS Channels

[13] The definition of the spectral response of the 2378 AIRS channels was provided using the 18 August 2002 instrument spectral response function (ISRF) version 1 from http://asl.umbc.edu/pub/airs/srf/. There have been small changes in the AIRS ISRF since then but they are small in terms of simulated radiances. This ISRF was also a good choice to compare with the observed radiances over the tropical ARM site.

[14] Some of the AIRS channels have been identified as bad for instrumental reasons and are often referred to as "popping" channels. The AIRS science team have identified a set of 276 channels which are bad and these were excluded from the comparison between the models and the AIRS observations. There were, in addition, a further 9 channels listed in Table 5 that were excluded from the analysis as they had obvious spikes when compared with all the models. These are probably also instrumental in origin but not yet included on the list of popping channels. The list of the "official" popping channels is available as part of the AIRS ISRF information.

[15] The 20 channels for transmittance and Jacobian comparisons were chosen because they are part of the 324 channel set distributed to NWP centres in real time, have different responses to temperature, water vapor and ozone and cover the complete spectrum. They are also high in information content as defined by degrees of freedom of signal [*Rodgers*, 1998] for NWP assimilation purposes.

3.3. Results Submitted

[16] The participants were requested to submit top of atmosphere equivalent black body brightness temperatures for all 2378 AIRS channels for 3 viewing angles, nadir, 45 and 60 degrees local zenith angles at the surface for the 52 diverse profiles described above. In addition, brightness temperatures for the one profile over the tropical ARM site (0.5S; 167E) at an incidence angle of 11degrees on 8 December 2002 were also requested to compare with the AIRS observed brightness temperatures.

[17] Optionally participants were also requested to provide, for the 20 AIRS channels defined in Table 3, layer to space transmittances and Jacobians scaled by a factor ΔX for changes in brightness temperature with respect to temperature, water vapor and ozone for all the 52 profiles.

Table 5. AIRS Channels Not on "Popping" List but Excluded From Comparison of Models With Observations

Channel Number	Frequency, cm^{-1}
326	743.80
342	748.88
415	772.94
432	778.77
571	837.53
919	967.43
923	969.04
1397	1300.30
1791	1561.63

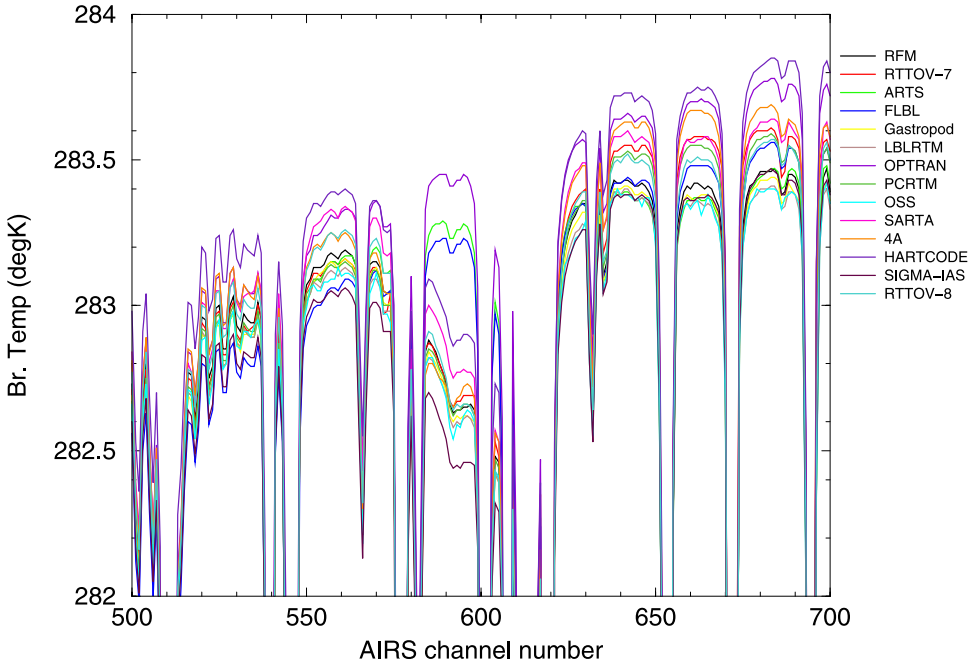

Figure 2. Comparison of AIRS RT models for the mean profile of the 52 set. The differences around channel 590 are due to the different treatment of CFCs in the different models.

For the models computing finite difference Jacobians the perturbations were defined as follows: (1) ±0.5K for the temperature Jacobians; (2) ±0.5% of the absorber layer mean mass mixing ratio.

[18] The comparisons were then made of the "scaled Jacobians", $\boldsymbol{J}$ defined as

$$\boldsymbol{J} = \mathbf{H} \times \Delta \mathrm{X} \tag{3}$$

where ΔX was +1 K for temperature and −1% of the absorber layer mean mass mixing ratio for water vapor and ozone. The remaining text will refer to $\boldsymbol{J}$ as a Jacobian for convenience even though this is not the true definition of a Jacobian defined in equation (2). Most of the models submitted results on the 100 layers between the levels defined in equation (1) but RTTOV-7 and σ-IASI were submitted on 43 and 60 layers respectively. To allow comparisons with other models, the transmittance profiles were linearly interpolated/extrapolated in pressure to the 101 levels. The Jacobians were remapped on to the 100 layers using the adjoint of the interpolation routine. This worked well for RTTOV-7 but the σ-IASI Jacobians remapped to 100 layers could not be reconciled with the other models for some profiles and channels and so the results for the σ-IASI Jacobians although included need to be treated with caution.

[19] For both the forward model comparisons and the Jacobians the results from each model were differenced with RFM, one of the line-by-line models, in order to be able to conveniently examine the intermodel differences. For the Jacobians the "measure of fit" adopted by *Garand et al.* [2001] was used defined as

$$M = 100 \times \sqrt{\frac{\sum \left(P_i - P_i^{ref}\right)^2}{\sum \left(P_i^{ref}\right)^2}} \tag{4}$$

where P_i is the profile variable at level i and P_i^{ref} is the reference profile variable which was taken to be the RFM Jacobian or transmittance profile for this study. For the results presented here P is either the level to space transmittance profile or the "scaled Jacobian" $\boldsymbol{J}$ as defined in equation (3). The summation over levels was restricted to the range 0.35–959 hPa (or the level above the surface if the surface pressure was less than 959 hPa) to avoid problems due to extrapolation above the top layer of RTTOV-7 and σ-IASI and interactions with the surface.

4. Forward Model Comparisons

4.1. Results for ECMWF Model Profiles

[20] As an illustration of the forward model comparisons, Figure 2 shows a portion of the spectrum from 810 to 880 cm^{-1} (channels 500–700) for the profile mean (number 52). Some differences between the different RT models are clear in this part of the spectrum. The obvious differences in the region of channel 590 (845 cm^{-1}) are due to the different way each model treats the absorption due to chlorofluorocarbons, CFCs, which in this case is CFC-11. There are also significant differences in the "window" regions between the lines due to differences in the water vapor continuum formulation. Those fast models which are based on a line-by-line model included in the study generally follow the model on which they were trained. For example, OSS follows LBLRTM closely. RTTOV-7, based on GENLN-2, which is similar to RFM, does follow RFM below 850 cm^{-1} (channel 600) but there are significant differences in the window regions at higher frequencies due to water vapor continuum differences between the GENLN2 run and the current version of RFM.

[21] To summarise the mean nadir view brightness temperature differences between each model and RFM Figures 3a and 3b show for all channels that the differences,

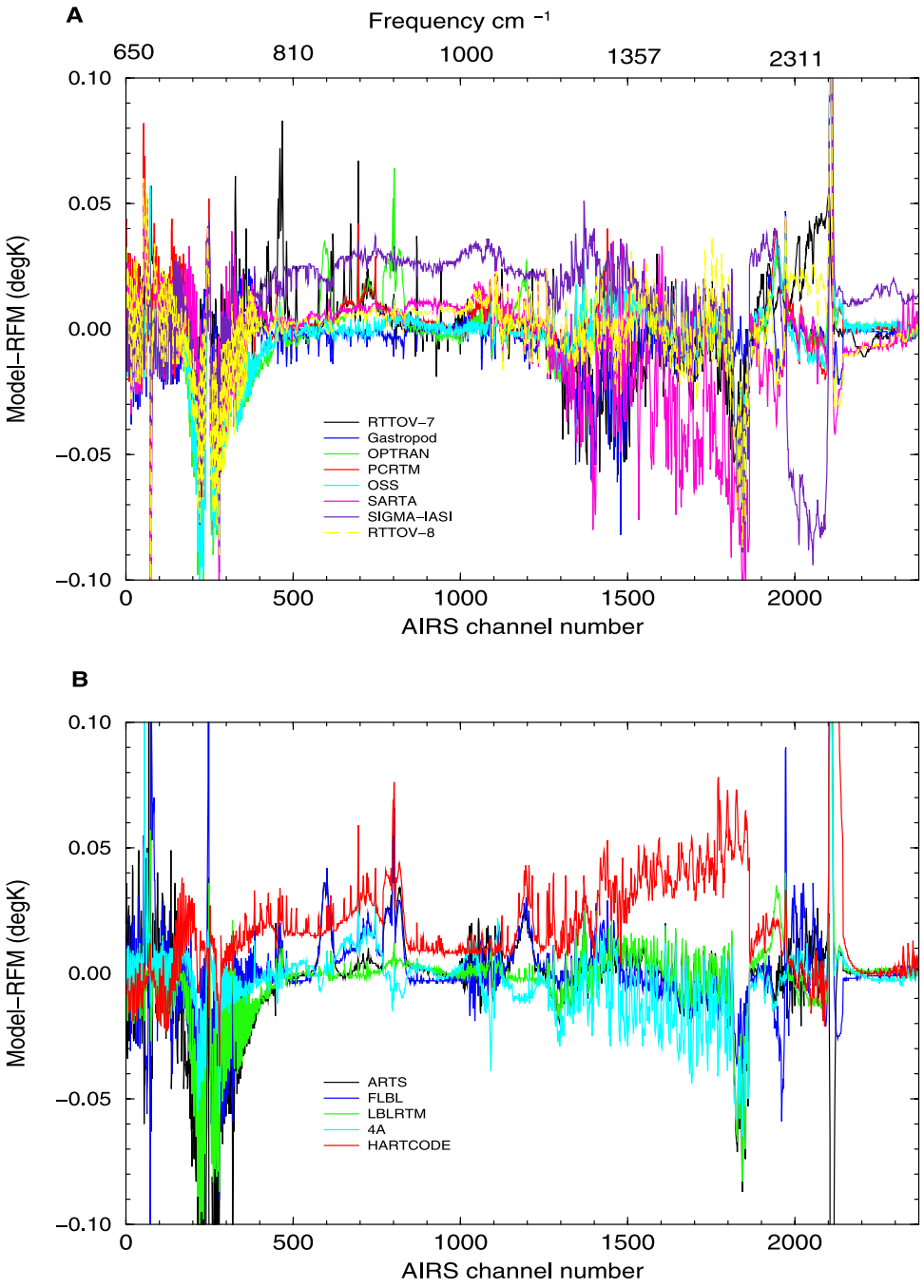

Figure 3. The mean difference from RFM for the 49 diverse profiles for all AIRS channels. (a) Fast models; (b) Line-by-line models.

Table 6. Comparison of all Models Simulated Brightness Temperatures With RFM[a]

	Nadir		45 degrees		60 degrees	
Model	Bias	Sdev	Bias	Sdev	Bias	Sdev
LBLRTM	0.01	0.04	0.01	0.05	0.01	0.05
4A	0.01	0.05	0.01	0.06	0.01	0.06
HARTCODE	0.02	**0.12**	0.02	**0.11**	0.02	**0.12**
SIGMA_IASI	0.02	**0.11**	0.02	**0.12**	**0.03**	**0.26**
ARTS	0.02	0.07	0.02	0.08	0.02	0.08
FLBL	0.01	0.05	0.01	0.06	0.02	0.07
Gastropod	0.01	0.05	0.01	0.05	0.01	0.06
OPTRAN	0.01	0.08	0.01	0.09	0.02	**0.11**
PCRTM	0.01	0.05	0.01	0.06	0.01	0.07
OSS	0.01	0.05	0.01	0.05	0.01	0.05
SARTA	0.02	0.08	0.02	0.09	0.02	0.09
RTTOV-7	0.01	0.06	0.01	0.07	0.02	0.08
RTTOV-8	0.01	0.07	0.01	0.08	0.02	0.08

[a]The differences are model-RFM in deg K and averaged over the 49 diverse profiles to form the mean and standard deviation (sdev) of the differences for each channel. The individual channel mean and standard deviation values are then all averaged to produce the numbers in the table. Bold numbers show values >0.02 K in bias and >0.1 K in standard deviation.

when averaged over the 49 profiles, are below the 0.1 K level except in a few narrow spectral bands. σ-IASI is slightly warmer (~0.05 K) than the other models in the atmospheric window and cooler in the shortwave CO_2 band. Hartcode has a warm bias in most parts of the spectrum except the "window" regions. SARTA generally has a cool bias in the water vapor band. It is important to bear in mind that these biases are with respect to the RFM model and not with respect to an absolute truth. RFM may not provide the best reference in all spectral regions. With a few exceptions, the differences of the models from RFM are similar. It is worth noting that the differences between line-by-line models (Figure 3b) are of the same order of magnitude as for the fast models (Figure 3a) suggesting that the different assumptions made in the spectroscopy and use of different line data sets dominate the RT model error statistics.

[22] To summarise the overall differences between models Table 6 gives the mean bias and standard deviation of the brightness temperature differences from RFM averaged over all the AIRS channels and the 49 diverse profiles. For all models except Hartcode the mean and standard deviation of the differences increase slightly with incident viewing angle but there is no great variation. Note all models assume a plane parallel atmosphere for these simulations and for 60 degrees at least this assumption introduces small biases (~0.2 K) with real data.

[23] The model differences are also compared over discrete spectral regions as plotted in Figure 4 and listed in Table 7 which represent areas of the spectrum used for temperature, water vapor, ozone or surface sounding. In terms of mean bias (not plotted) most differences are below ±0.02 K, but most models depart from RFM in the 2350–2420 cm^{-1} band being warmer except ARTS. Many models have a cool bias (~0.01 K) for the longwave CO_2 bands relative to RFM. Both Hartcode and σ-IASI exhibit larger biases for most bands relative to RFM than other models with the 2350–2420 cm^{-1} band in particular for Hartcode showing a large positive mean bias of greater than 0.1 K and standard deviation of 0.5 K. In addition, Figure 4 shows the AIRS instrument noise for each of the bands which is greater than the model differences with the exception of the 2350–2420 cm^{-1} band. This is encouraging as it suggests the RT models are on average accurate enough for forward calculations of AIRS radiances. However over

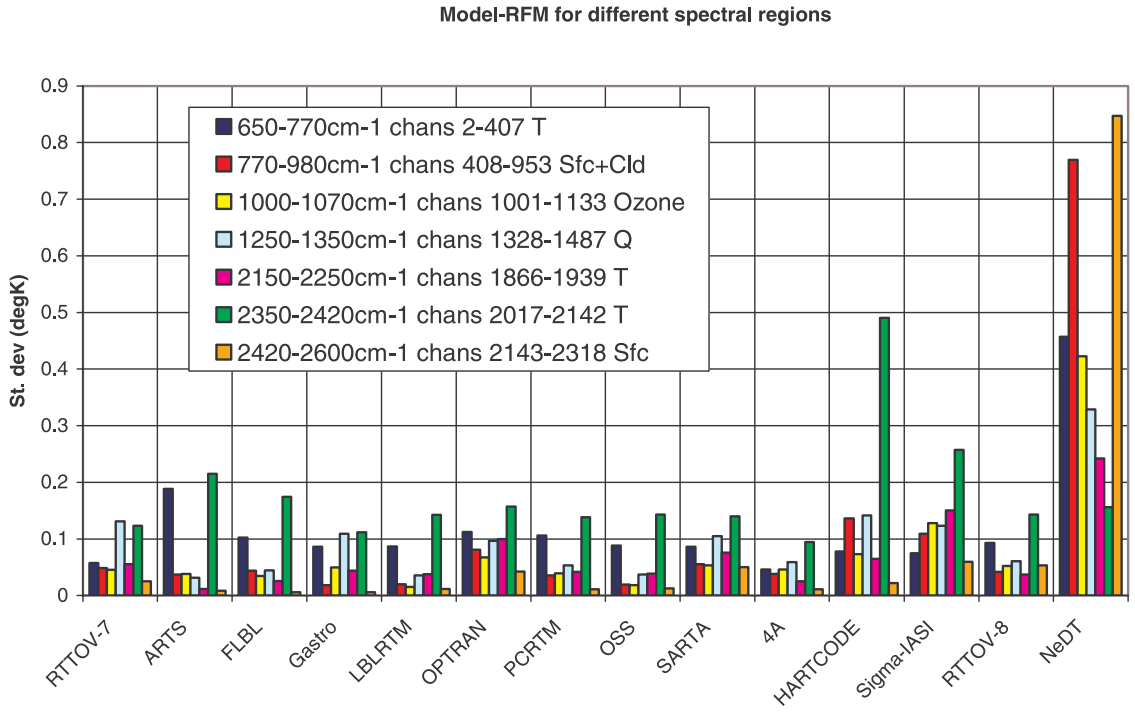

Figure 4. A histogram of the RT model nadir view differences from RFM for different spectral regions. The columns on the far right give the AIRS instrument noise for a 250 K brightness temperature scene.

Table 7. Comparison of Model-RFM Brightness Temperature Differences for Several Spectral Regions[a]

Frequency Range cm^{-1}	RTTOV 7	ARTS	FLBL	Gastropod	LBLRTM	OPTRAN	PCRTM	OSS	SARTA	4A	HART-CODE	Sigma- IASI	RTTOV 8
650–770	0.009	**−0.031**	−0.010	−0.006	−0.016	−0.017	−0.007	−0.017	−0.002	−0.002	0.005	−0.006	−0.008
Temp	0.058	**0.189**	**0.102**	0.086	0.087	**0.112**	**0.106**	0.088	0.086	0.046	0.078	0.075	0.093
770–980	0.007	0.006	0.008	−0.002	0.000	0.006	0.004	0.000	0.007	0.003	**0.021**	**0.025**	0.004
Sfc + Cloud	0.048	0.037	0.044	0.018	0.020	0.081	0.036	0.020	0.055	0.038	**0.136**	**0.109**	0.042
1000–1070	0.005	0.003	0.000	0.001	0.000	0.002	0.005	0.000	0.010	0.000	0.010	**0.031**	0.009
Ozone	0.045	0.038	0.035	0.049	0.015	0.068	0.039	0.018	0.053	0.046	0.073	**0.128**	0.052
1250–1350	**−0.026**	0.002	0.008	**−0.023**	0.004	0.006	0.008	0.004	−0.018	−0.005	**0.027**	**0.025**	−0.004
Water Vap	**0.131**	0.032	0.044	**0.109**	0.036	0.097	0.053	0.037	**0.105**	0.059	**0.141**	**0.123**	0.061
2150–2250	0.010	0.001	−0.001	0.003	0.008	0.002	0.007	0.008	−0.010	−0.005	0.015	**0.031**	0.000
Temp	0.055	0.012	0.025	0.044	0.038	**0.100**	0.042	0.039	0.076	0.025	0.065	**0.150**	0.037
2350–2420	**0.025**	**−0.040**	0.023	0.011	**0.025**	**0.026**	**0.020**	**0.025**	0.004	**0.020**	**0.108**	0.000	0.014
Temp	**0.123**	**0.215**	**0.175**	**0.112**	**0.143**	**0.157**	**0.138**	**0.143**	**0.140**	0.095	**0.490**	**0.257**	**0.143**
2420–2600	−0.004	0.001	−0.001	−0.001	0.001	0.001	0.000	0.001	−0.007	−0.001	0.003	0.013	−0.007
Surface	0.025	0.009	0.006	0.006	0.011	0.042	0.011	0.013	0.050	0.011	0.022	0.059	0.053

[a]Upper number: bias; lower number: standard deviation. Larger differences are highlighted in bold.

narrow spectral regions as shown in Figure 3 it may still be the case that the RTM errors may exceed the instrument noise.

4.2. Comparison With AIRS Measurements

[24] The comparison with observed AIRS radiances was made for one profile over the tropical western Pacific ARM site as described in section 3.1. The results are shown in Figures 5a and 5b and the first thing to note is the much greater difference between models and observations than between models and models shown in Figure 3, with differences from the observations typically up to ±1 K and in some spectral regions up to ±3 K. All models show a negative difference of 2–3 K with respect to the AIRS observations around the 9.8 micron ozone band (channels 1023–1153), suggesting that the ozone profile from the ECMWF model is in error. High-peaking CO_2 bands (channels 1–406, 1912–2121) also have consistent differences across all models again probably due to errors in the ECMWF upper stratospheric temperature profile. Table 8 summarizes the differences showing that SARTA has the best agreement with the AIRS observations in terms of root mean square difference and this is clear around AIRS channel 2150 which is due to the improved CO_2 R-branch line mixing formulation in kCARTA and also a new water vapor continuum. Table 8 shows the cool biases of most of the models can be attributed to the deficiencies in the profile as shown by the statistics which exclude the ozone and high-peaking CO_2 bands. The RMSD values of all models are also reduced, especially for SARTA, when these bands are excluded from the statistics. The good fit of SARTA is not surprising as the spectroscopic parameters it uses (e.g., gaseous absorption coefficients, water vapor continuum) were tuned on an AIRS radiosonde match-up data set that included this profile (see *Strow et al.* [2006], for more details). RFM the reference model for this study agrees reasonably well except at the CO_2 4.3 μm band edge and at the peak of the CO_2 15 μm band and so this needs to be noted for the comparisons with RFM in section 4.1. Notable departures from the observations for the other models seen in Figures 5a and 5b include several cool biases at discrete frequencies for OPTRAN and ARTS which have two significant negative biases of −8K at 4.18 μm close to the band edge and at 13.9 μm. Hartcode differences from the observations show a large warm peak on the CO_2 4.3 μm band edge.

5. Comparison of Layer to Space Transmittances and Jacobians

5.1. Layer to Space Transmittances

[25] Profiles of layer to space transmittance were computed by some of the RT models for the 52 profiles and the 20 AIRS channels as indicated in Table 3. The results are summarized in Table 9 as the mean transmittance difference from RFM computed using equation (4) for each profile and then averaged over the 49 diverse profiles. There are a few channels from the set which are modeled less consistently compared to RFM, i.e., 71, 77 and 2107 and these channels are all close to strong CO_2 absorption bands. As both line-by-line and fast models exhibit differences this is likely to be due to spectroscopic differences rather than fast model problems. Also worth noting are the larger differences for the 4A model for most of the water vapor and shortwave infrared channels. For some of the AIRS water vapor channels (1766, 1812) RTTOV-8 transmittances also depart from RFM more than the other models.

5.2. Jacobians

[26] An example of the temperature Jacobians computed is shown in Figure 6a. For this profile, in general the models are in good agreement. Figure 7 summarizes the fit for temperature Jacobians for temperature sensitive channels. These box and whisker plots show both the range and mean/median of the fit to RFM for all 49 profiles. Some channels have better fits (e.g., 77) than others (e.g., 787) and some channels have worse fits between models (e.g., 71).

[27] The first point to note is that for some of the channels the σ-IASI deviations from the RFM Jacobians are large and this is due to the resampling of the 60 level values supplied to 100 levels to enable comparisons to be made. For channel 787, a window channel, both OPTRAN and FLBL seem to have problems computing a Jacobian for this weak absorption domain as the fit to RFM is poor for most profiles.

[28] The goodness of fit values are a useful metric to assess the overall performance of the models. However they do not show more subtle problems in computed Jacobians which could be detrimental to retrieval and data assimilation

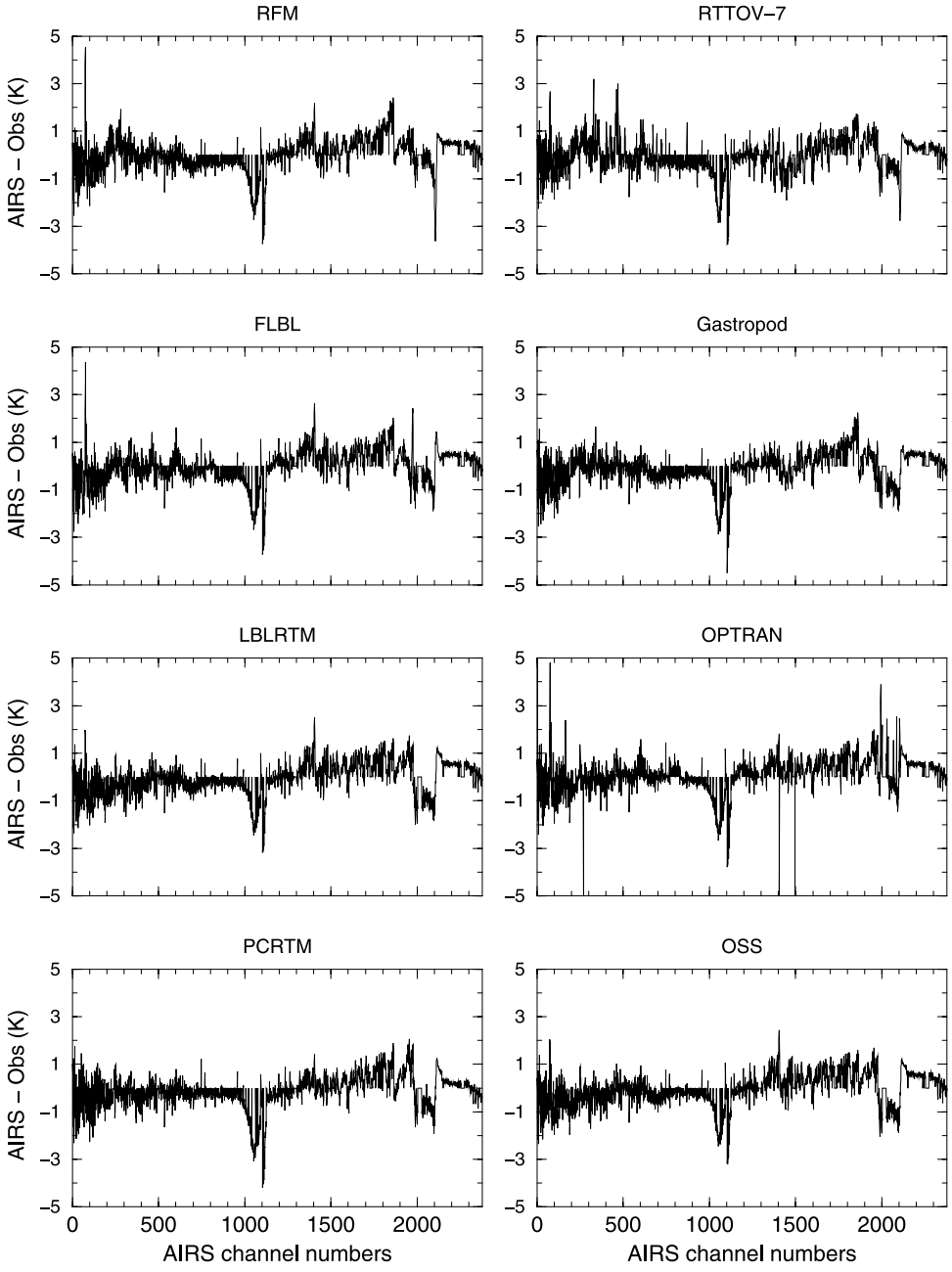

Figure 5a. The difference between each model and AIRS observations over the tropical ARM site on 8 December 2002 for a surface incidence angle of 11 degrees.

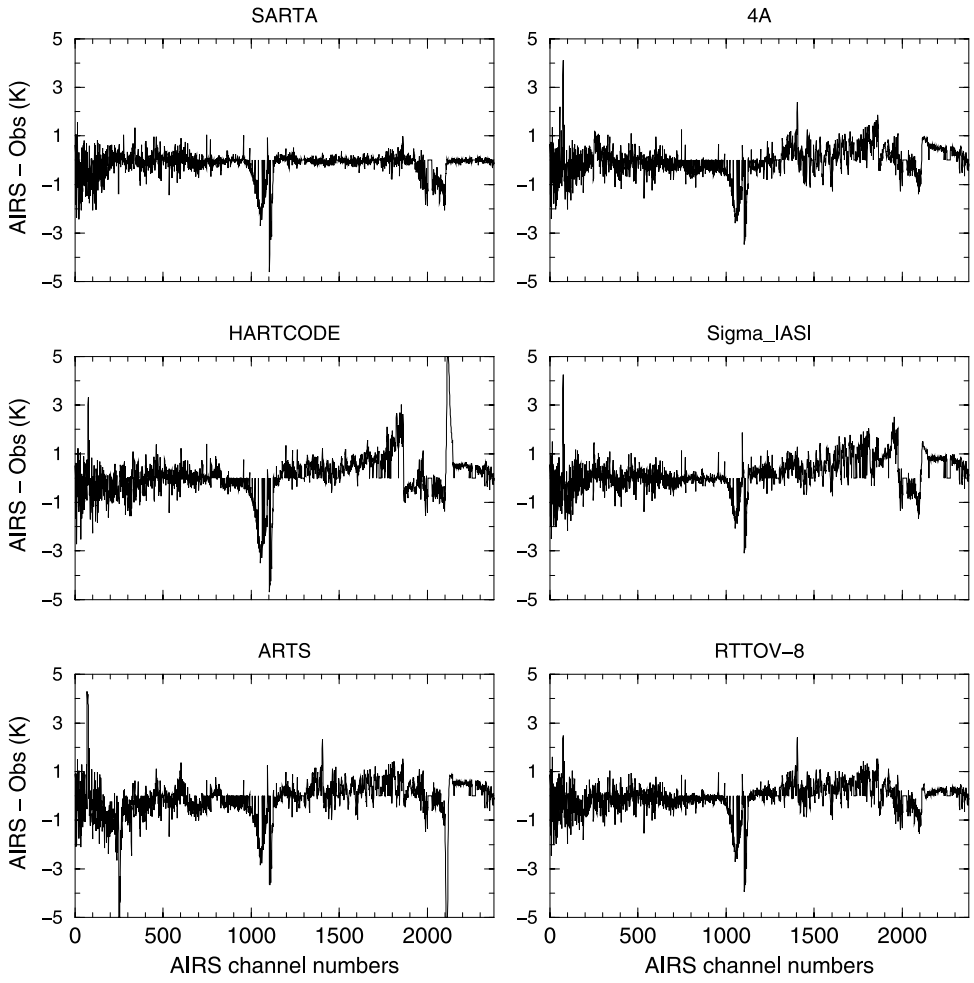

Figure 5b. As in Figure 5a.

applications. One example for channel 787 is shown in Figure 6b which the majority of the models show as a weak smooth peak in the temperature Jacobian close to the ground (~800 hPa). Some models however have a more variable structure in the vertical (e.g., 4A, PCRTM) which are obviously unphysical. The issue this comparison is unable to resolve is whether these features matter for assimilation/retrievals as it is a relatively weak Jacobian in terms of absolute temperature changes.

[29] Figure 8 shows the box and whisker plots for the water vapor Jacobians and again the sigma-IASI results should be treated with caution. In general the accuracy of AIRS water vapor Jacobians were poorest for cold, dry profiles. In particular, Gastropod and RTTOV-7 showed poor performance for these profiles in channels 672 and 1142 (associated with extrapolation of the fast model regression bounds in the case of the Gastropod model), and the poorer fits for FLBL in channels 1437 and 1449 also appear to be associated with profiles with high surface elevation over Antarctica. However, some poor fits to RFM Jacobians appear likely to be associated with differences in spectroscopy, e.g., the systematic difference in model Jacobians in channel 453, and poor fits (and associated significant differences in simulated transmittances) for RTTOV-8 Jacobians in channel 1766 and RTTOV-7 in channel 1812.

Table 8. Model Minus AIRS Observed Brightness Temperature Differences Averaged Over All Nonpopping Channels for the Tropical ARM Profile and for Those Excluding Ozone and High-Peaking CO_2 Channels[a]

	All Valid Channels		No Ozone and Strong CO_2	
Model	Mean deg K	RMSD deg K	Mean deg K	RMSD deg K
RFM	0.02	0.75	0.18	0.57
RTTOV7	−0.07	0.75	0.03	0.59
RTTOV8	−0.06	0.64	0.13	0.44
FLBL	−0.01	0.75	0.20	0.58
Gastropod	−0.09	0.71	0.10	0.52
LBLRTM	−0.05	0.72	0.18	0.54
OPTRAN	0.11	0.82	**0.27**	0.59
PCRTM	−0.13	0.74	0.04	0.48
OSS	−0.05	0.72	0.18	0.54
SARTA	−0.19	0.57	−0.02	0.23
4A	−0.03	0.68	0.10	0.53
HARTCODE	0.09	0.96	**0.36**	**0.75**
SIGMA_IASI	0.22	0.76	**0.38**	**0.64**
ARTS	−0.16	0.98	0.12	0.51

[a]The bold figures are for mean differences >0.2 K and standard deviation >0.6 K. ARM: Atmospheric Radiation Measurement.

Table 9. Mean Transmittance Differences From RFM Using Goodness of Fit Formula (Equation (2))[a]

AIRS Channel	Gastropod	PCRTM	Optran	4A	FLBL	RTTOV-8	RTTOV-7	Sigma-IASI
71	6.42E-03	3.79E-02	2.12E-02	**2.50E-01**	2.12E-03	5.29E-03	6.64E-03	**5.02E-02**
77	**1.18E-01**	**2.94E-01**	5.44E-03	**9.32E-01**	**2.19E-01**	**1.49E-01**	2.65E-02	5.00E-02
305	8.23E-03	8.07E-03	1.11E-02	3.12E-02	1.06E-02	1.23E-02	1.82E-04	2.04E-03
453	4.29E-05	4.96E-04	1.02E-03	1.01E-02	1.00E-03	3.88E-04	1.93E-03	6.06E-04
672	2.19E-03	7.73E-04	1.42E-03	6.97E-03	1.79E-03	9.67E-04	1.92E-02	7.53E-04
787	1.22E-05	6.06E-04	5.87E-03	3.00E-03	4.79E-03	1.28E-03	1.45E-04	1.39E-03
1021	1.09E-03	5.35E-04	7.84E-04	2.53E-03	2.45E-04	1.77E-03	1.25E-03	4.81E-03
1090	6.28E-03	4.12E-03	3.97E-03	**1.06E-01**	5.55E-03	4.88E-03	2.96E-03	1.86E-02
1142	1.24E-03	5.92E-05	4.69E-04	7.62E-03	1.10E-03	8.43E-04	1.64E-03	1.33E-03
1437	2.95E-03	2.56E-03	1.99E-03	4.14E-02	1.96E-03	4.76E-04	1.17E-02	4.77E-03
1449	1.80E-03	2.72E-03	2.37E-03	**5.76E-02**	9.27E-04	4.27E-04	1.28E-02	3.72E-03
1627	1.33E-03	3.12E-04	2.18E-04	**1.25E-01**	6.67E-04	2.24E-03	1.98E-03	1.56E-03
1766	8.80E-04	4.67E-04	8.98E-05	**1.12E-01**	4.08E-06	**8.67E-02**	8.43E-03	6.71E-03
1794	4.27E-04	7.29E-04	5.96E-04	**1.42E-01**	3.35E-04	2.30E-03	1.64E-02	4.93E-03
1812	3.34E-03	1.71E-03	1.37E-03	**6.58E-02**	1.34E-03	1.69E-02	1.62E-02	7.77E-03
1917	2.21E-03	2.58E-03	2.63E-03	3.71E-02	4.71E-04	2.53E-04	5.23E-03	2.95E-02
1958	1.74E-03	7.86E-03	3.28E-03	**1.02E-01**	3.86E-03	5.03E-03	3.20E-04	1.92E-02
1995	8.95E-03	5.82E-03	1.28E-03	**1.18E-01**	4.20E-03	2.88E-03	1.91E-03	2.02E-02
2107	**1.41E-01**	**1.88E-01**	**2.17E-01**	2.39E-02	**2.91E-01**	**1.15E-01**	1.82E-03	**2.36E-01**
2197	0.00E+00	8.98E-05	9.80E-05	3.61E-04	0.00E+00	1.82E-03	1.38E-03	7.14E-05

[a]The transmittance is in units from 0–1, and differences greater than 0.05 are highlighted in bold.

[30] Finally for ozone Jacobians Figure 9 summarizes the fit to RFM for the 2 selected channels. PCRTM has the best fit to RFM for ozone but most models have good fits compared with the water vapor Jacobians. RTTOV-7 departs from the reference more at the peak of the Jacobian but this may be due to the 43 levels on which the computation is done compared with 100 levels for the other models rather than inaccuracies in the model itself.

[31] The results above all refer to Jacobians computed for nadir views. Computations were also made for viewing angles of 45 and 60 degrees. The results were all similar to the nadir view Jacobians presented here and so viewing angle does not appear to be a factor which affects the Jacobian errors significantly.

6. Summary

[32] Results of comparisons of AIRS radiative transfer models are presented here in order to better understand the error characteristics of AIRS RT models important for data assimilation and retrieval applications using AIRS data. For the forward model comparisons when averaged over 49 profiles all the models agree within 0.06 K and most models to within 0.02 K of the RFM model used as a reference. Exceptions to this are in regions affected by CFCs, water vapor continuum or CO_2 line mixing where larger differences can be found. The differences between the line-by-line models are as large as between the fast models suggesting the dominant error sources are related to the spectroscopic assumptions and line parameters used rather than the fast model formulations. Other possible sources of error include the treatment of the surface reflection, Plank constants assumed, and treatment of layers in the integration of the radiative transfer equation.

[33] The mean biases shown by each model can be removed by a bias correction procedure as is standard practice in data assimilation applications (although there will be associated, uncorrected Jacobian errors). It is encouraging that the standard deviation of the differences between the models and RFM is for all models less than the AIRS instrument noise. This suggests that the forward model error is not the dominant error source but instrument noise and errors of representativity are likely to be more important when comparing simulated with measured radiances.

[34] The comparison against AIRS observations for a single profile shows bigger differences with mean brightness temperature differences at the 1 K level. The SARTA model fits the AIRS observations best especially in the 2100–2200 cm^{-1} region but has been tuned using data including this profile. Some of the differences with the AIRS observations are due to our inadequate representation of the atmospheric state for ozone and stratospheric variables.

[35] In terms of transmittances the 4A model, and to a lesser extent RTTOV-8, are consistently different from RFM but this may just reflect the fact that these models have recently been updated and include more up to date spectroscopy than RFM. The performance of the models in terms of Jacobian accuracy varies with most models having problems for some profiles. For temperature the AIRS 917 cm^{-1} channel appears to be the most problematic channel for modeling Jacobians with 4 out of the 8 models diverging significantly from RFM. For water vapor RTTOV-8 is consistently different from the RFM response for most water vapor channels but this may be due to the new spectroscopy in the kCARTA data set on which this version of RTTOV-8 was trained. The ozone Jacobians were in general more consistent between models. Further study is needed to assess the impact of model-specific Jacobian errors (e.g., erratic weak Jacobians, poorly modeled Jacobians in cold, dry atmospheres) and Jacobian errors associated with bias correction, on retrieval accuracy. *Sherlock* [2005] has started to address this with a study of the effect of fast model errors, including Jacobians, on AIRS retrieval accuracies.

[36] To allow other modelers who did not participate in this comparison to compare their models with the data sets

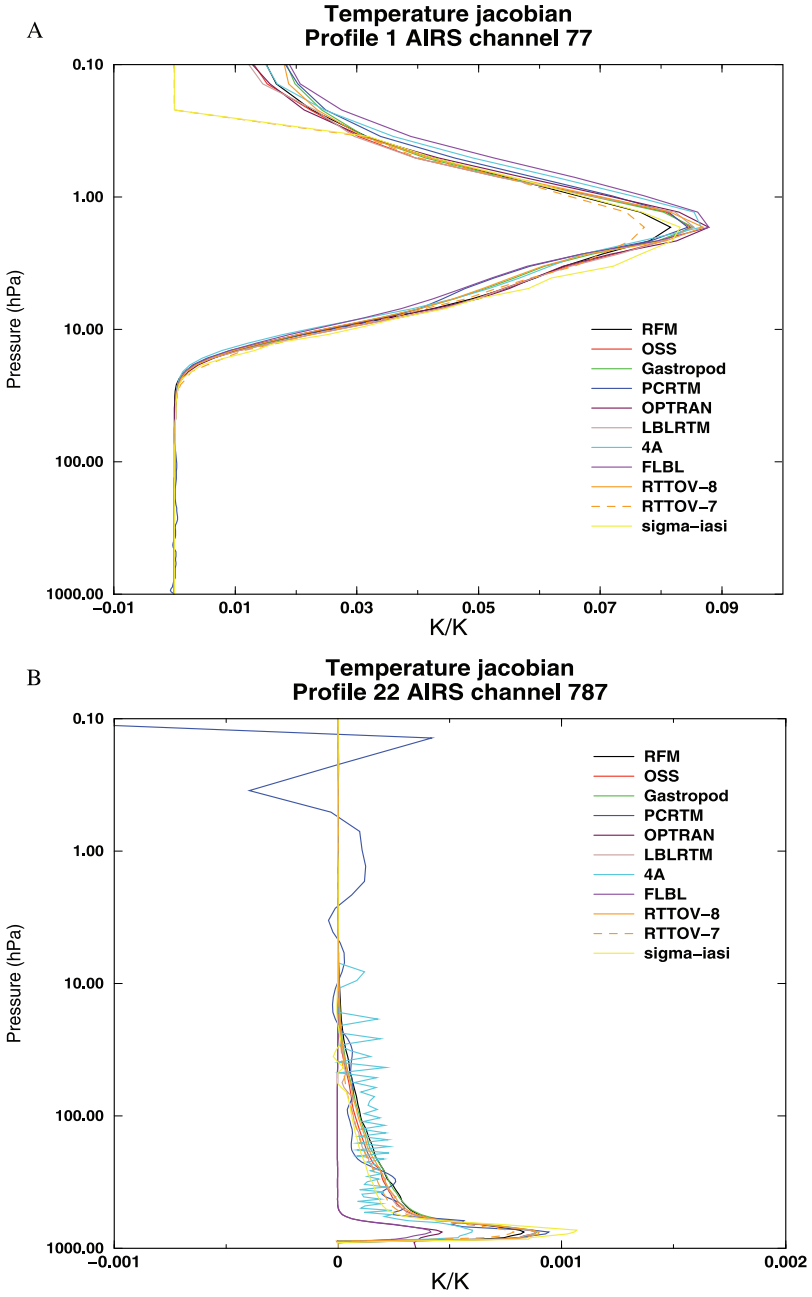

Figure 6. (a) An example of the temperature Jacobian comparison for profile 1 and AIRS channel 77 and (b) a temperature Jacobian for profile 22 and channel 787.

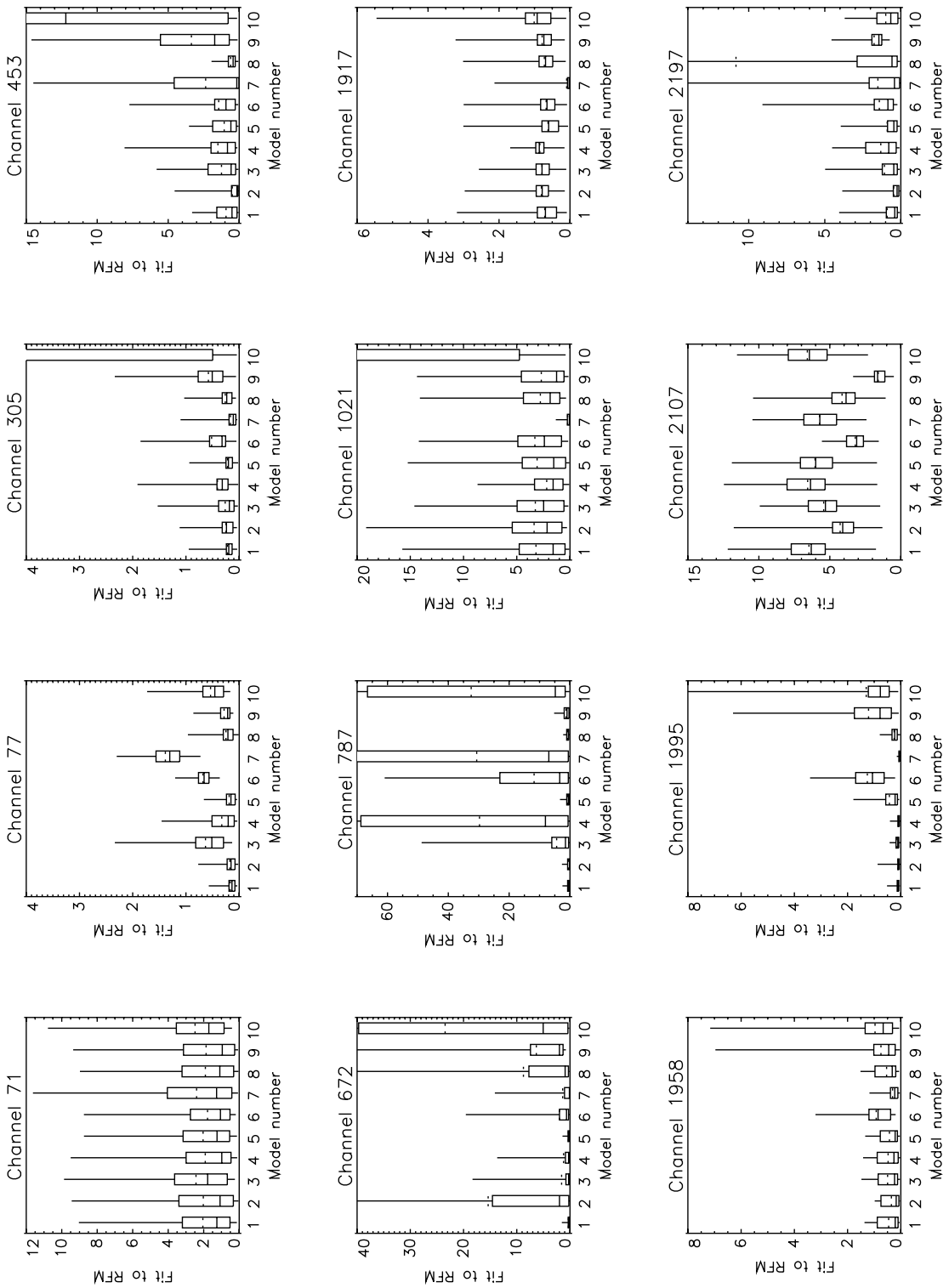

Figure 7. Box and whisker plots which show the range of the fits to the RFM temperature Jacobians as defined in equation (2) for each model. The box gives the bounds of the upper and lower quartiles, the solid line through the box is the median, the dashed line is the average, and the whiskers indicate the maxima and minima of the differences.

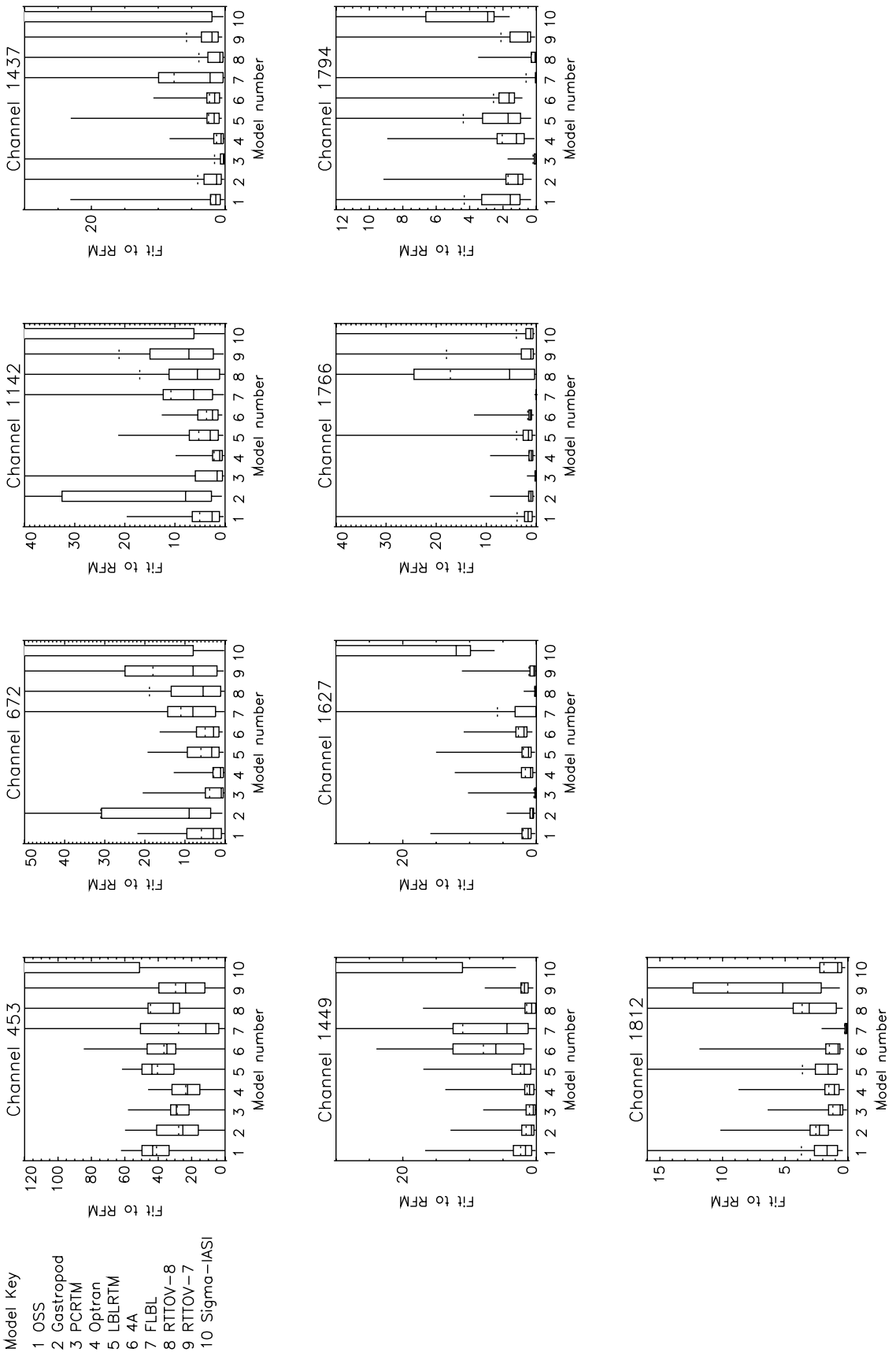

Figure 8. As in Figure 7 for the water vapor Jacobians.

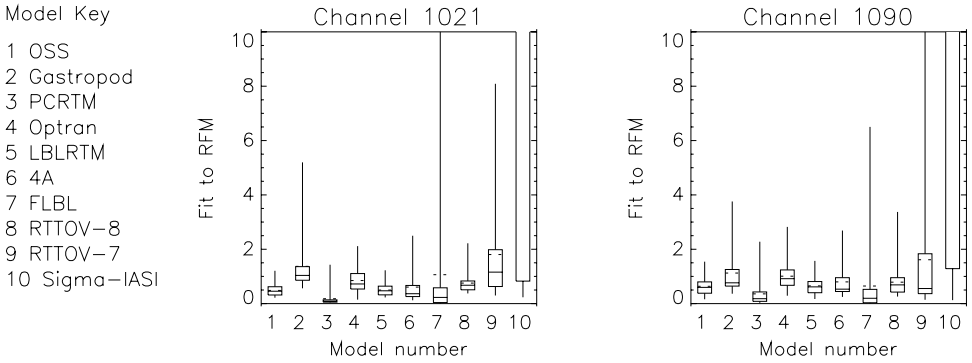

Figure 9. As in Figure 7 for the ozone Jacobians.

presented in this paper the International TOVS Working Group have set up a web site which includes the raw model output data that produced the results presented here. The link is at: http://cimss.ssec.wisc.edu/itwg/groups/rtwg/rtairs.html.

[37] **Acknowledgments.** The support of Anu Dudhia (University of Oxford) in making the RFM available for this study is gratefully acknowledged. Also the International TOVS Working Group is acknowledged for providing the Web site to coordinate the comparison.

References

Amato, U., G. Masiello, C. Serio, and M. Viggiano (2002), The sigma-IASI code for the calculation of infrared atmospheric radiance and its derivatives, *Environ. Modell. Software*, *17*(7), 651–667.

Andersson, E., J. Pailleux, J.-N. Thepaut, J. R. Eyre, A. McNally, G. A. Kelly, and P. Courtier (1994), Use of cloud-cleared radiances in three/four-dimensional variational data assimilation, *Q. J. R. Meteorol. Soc.*, *120*, 627–653.

Buehler, S. A., P. Eriksson, T. Kuhn, A. von Engeln, and C. Verdes (2005), ARTS, The Atmospheric Radiative Transfer Simulator, *J. Quant. Spectrosc. Radiat. Transfer*, *91*, 65–93.

Chevallier, F. (2001), Sampled databases of 60 level atmospheric profiles from the ECMWF analyses, report, Met Off., Devon, U.K. (Available at http://www.metoffice.gov.uk/research/interproj/nwpsaf/rtm/profiles.pdf)

Chevallier, F., A. Chedin, F. Cheruy, and J. J. Morcrette (2000), TIGR-like atmospheric-profile databases for accurate radiative-flux computation, *Q. J. R. Meteorol. Soc.*, *126*, 777–785.

Clough, S. A., M. J. Iacono, and J. L. Moncet (1992), Line-by-line calculation of atmospheric fluxes and cooling rates: 1. Application to water vapor, *J. Geophys. Res.*, *97*, 15,761–15,780.

DeSouza-Machado, S., L. L. Strow, D. Tobin, H. Motteler, and S. E. Hannon (1999), Improved atmospheric radiance calculations using P/R-branch line mixing, paper presented at the EOS/SPIE Symposium on Aerospace Remote Sensing, Int. Soc. for Opt. Eng. (SPIE), Florence, Italy, 20 Sept.

English, S. J., R. J. Renshaw, P. C. Dibben, A. J. Smith, P. J. Rayer, C. Poulsen, F. W. Saunders, and J. R. Eyre (2000), A comparison of the impact of TOVS and ATOVS satellite sounding data on the accuracy of numerical weather forecasts, *Q. J. R. Meteorol. Soc.*, *126*, 2911–2931.

Garand, L., et al. (2001), Radiance and Jacobian intercomparison of radiative transfer models applied to HIRS and AMSU channels, *J. Geophys. Res.*, *106*(D20), 24,017–24,031.

Hoke, M. L., S. A. Clough, W. J. Lafferty, and B. J. Olson (1989), Line coupling in oxygen and carbon dioxide, in *Proceedings of IRS 1988, Lille, France*, edited by J. LeNoble and J.-F. Geleyn, pp. 368–371, A. Deepak, Hampton, Va.

Liu, X., W. L. Smith, D. K. Zhou, and A. Larar (2006), Principal component-based radiative transfer model for hyper-spectral sensors: Theoretical concept, *Appl. Opt.*, *45*(1), 201–209.

McMillin, L. M., X. Xiong, Y. Han, T. J. Kleespies, and P. Van Delst (2005), Atmospheric transmittance of an absorbing gas. 7. Further improvements to the OPTRAN approach, *Appl. Opt.*, *45*(9), 2028–2034.

Miskolczi, F., R. Rizzi, R. Guzzi, and M. Bonzagni (1989), A new high resolution atmospheric transmittance code and its application in the field of remote sensing, in *IRS '88: Current Problems in Atmospheric Radiation*, vol. 121, A. Deepak, Hampton, Va.

Moncet, J.-L., G. Uymin, and H. E. Snell (2004), Atmospheric radiance modeling using the optimal spectral sampling (OSS) method, *Proc. SPIE Int. Soc. Opt. Eng.*, *5425*, 368–374.

Rodgers, C. D. (1998), Information content and optimisation of high spectral resolution remote measurements, *Adv. Space Res.*, *21*(3), 361–367.

Rodriguez, R., et al. (1999), Model, software, and data-base for computation of line-mixing effects in infrared Q branches of atmospheric CO_2. I. Symmetric isotopomers, *J. Quant. Spectrosc. Radiat. Transfer*, *6*, 153–184.

Saunders, R. W., M. Matricardi, and P. Brunel (1999), An improved fast radiative transfer model for assimilation of satellite radiance observations, *Q. J. R. Meteorol. Soc.*, *125*, 1407–1426.

Scott, N. A., and A. Chedin (1981), A fast line-by-line method for atmospheric absorption computation: The Automated Atmospheric Absorption Atlas, *J. Appl. Meteorol.*, *20*, 802–812.

Sherlock, V. (2005), Extended studies with the IASI_1DVar code to characterize the impact of AIRS fast model errors on AIRS retrieval accuracy, Eur. Org. for the Exploit. of Meteorol. Satell., Darmstadt, Germany. (Available at http://www.eumetsat.int/Home/Main/What_We_Do/SAFs/The_Network/Visiting_Scientists_Programme/SP_1121420805375?l=en)

Sherlock, V., A. Collard, S. Hannon, and R. W. Saunders (2003), The Gastropod Fast Radiative Transfer Model for advanced infrared sounders and characterization of its errors for radiance assimilation, *J. Appl. Meteorol.*, *42*(12), 1731–1747.

Soden, B., et al. (2000), An intercomparison of radiation codes for retrieving upper-tropospheric humidity in the 6.3 micron band: A report from the first GVaP workshop, *Bull. Am. Meteorol. Soc.*, *81*(4), 797–808.

Strow, L. L., D. Tobin, and S. Hannon (1994), A compilation of first order line mixing coefficients for CO_2 Q branches, *J. Quant. Spectros. Radiat. Transfer*, *52*, 281–294.

Strow, L. L., H. E. Motteler, R. G. Benson, S. E. Hannon, and S. De Souza-Machado (1998), Fast computation of monochromatic infrared atmospheric transmittances using compressed look-up tables, *J. Quant. Spectrosc. Radiat. Transfer*, *59*, 481–493.

Strow, L. L., S. E. Hannon, S. De Souza-Machado, H. E. Motteler, and D. Tobin (2003), An overview of the AIRS Radiative Transfer Model, *IEEE Trans. Geosci. Remote Sens.*, *41*(2), 303–313.

Strow, L. L., S. E. Hannon, S. De-Souza Machado, H. E. Motteler, and D. Tobin (2006), Validation of the atmospheric infrared sounder radiative transfer algorithm, *J. Geophys. Res.*, *111*, D09S06, doi:10.1029/2005JD006146.

Tjemkes, S. A., et al. (2003), ISSWG line-by-line inter-comparison experiment, *J. Quant. Spectrosc. Radiat. Transfer*, *77*, 433–453.

Turner, D. S. (1995), Absorption coefficient estimation using a two-dimensional interpolation procedure, *J. Quant. Spectrosc. Radiat. Transfer*, *53*(6), 633–637.

Xiong, X., and L. M. McMillin (2005), Alternative to the effective transmittance approach for the calculation of polychromatic transmittances in rapid transmittance models, *Appl. Opt.*, *44*, 67–76.

N. Bormann, European Centre for Medium Range Weather Forecasts, Shinfield Park, Reading, RG2 9AX, UK.

P. Brunel, MétéoFrance, CMS, BP147, Lannion 22302, France.

Y. Han, NOAA, 5200 Auth Road, Camp Springs, MD 20746-4304, USA.

S. Hannon and L. Strow, Department of Physics, University of Maryland, Baltimore County, 1000 Hilltop Circle, Baltimore, MD 21250, USA.

S. Heilliette, CNRS, Laboratoire Meteorologie Dynamique, Palaiseau, 91128, France.

X. Liu and F. Miskolczi, MS 401A Atmospheric Sciences Competency, NASA Langley Research Center, Hampton, VA 23681, USA.

G. Masiello, IMAA-CNR, Tito Scalo, Potenza, 85050, Italy.

J.-L. Moncet and G. Uymin, Atmospheric and Environmental Research, 131 Hartwell Avenue, Lexington, MA 02421-3126, USA.

P. Rayer and R. Saunders, Met Office, Exeter, EX1 3PB UK.

V. Sherlock, National Institute of Water and Atmospheric Research, Private Bag 14-901, Wellington, New Zealand.

D. S. Turner, Environment Canada, 4905 Dufferin Street, Toronto, ON, Canada, M3H 5T4.

A. von Engeln, Institute of Environmental Physics, Bremen University, 28334 Bremen, Germany.